



Universiteit
Leiden
The Netherlands

Automated analysis of 3D echocardiography

Stralen, M. van

Citation

Stralen, M. van. (2009, February 25). *Automated analysis of 3D echocardiography*. *ASCI dissertation series*. Retrieved from <https://hdl.handle.net/1887/13521>

Version: Corrected Publisher's Version

License: [Licence agreement concerning inclusion of doctoral thesis in the Institutional Repository of the University of Leiden](#)

Downloaded from: <https://hdl.handle.net/1887/13521>

Note: To cite this publication please use the final published version (if applicable).

Cover Page



Universiteit Leiden



The handle <http://hdl.handle.net/1887/13521> holds various files of this Leiden University dissertation.

Author: Stralen, M. van

Title: Automated analysis of 3D echocardiography

Issue date: 2009-02-25

Automated tracking of the mitral valve annulus motion in apical echocardiographic images using multidimensional dynamic programming

3

WE DEVELOPED A SEMI-AUTOMATIC method for tracking the mitral valve annulus (MVA) in echocardiographic images, in particular, tracking the septal and the lateral mitral valve hinge points.

The algorithm is based on multidimensional dynamic programming combined with apodized block matching. The method was tested on single-beat apical four chamber image sequences of 20 patients with acute myocardial infarction. The automated tracking results were evaluated by comparing them with the average manual tracking results of two experts. The mitral valve hinge point displacements and the total mitral excursions obtained by the automatic technique agreed well with those obtained manually and outperformed two commonly used tracking methods (forward tracking and minimum tracking).

In conclusion, this novel semi-automatic tracking method is clinically valuable and capable of tracking the MVA motion within the limits of interobserver variability. The technique is robust, even in low frame rate, redigitized VCR images of clinical quality.

This chapter has been derived from © 2007, with permission from Elsevier):

Automated tracking of the mitral valve annulus motion in apical echocardiographic images using multidimensional dynamic programming. S.T. Nevo, M. van Stralen, A.M. Vossepoel, J.H.C. Reiber, N. de Jong, A.F.W. van der Steen and J.G. Bosch. *Ultrasound Med Biol* 2007; 33(9): 1389-1399.

3.1 | Introduction

mitral valve annulus motion Analysis of the mitral valve annulus (MVA) movement is useful in the evaluation of global and regional left ventricular (LV) function and is important for diagnosis of mitral annular diseases and LV disorders [Eto et al. 2005; Pai et al. 1991; Willenheimer et al. 1999] In addition, the motion of the MVA plane contributes significantly to the left ventricular volume change over the cardiac cycle and correlates well with LV ejection fraction [Eto et al. 2005].

the purpose Echocardiography is a non-invasive and low cost technique for evaluating LV function, but it is not an easy modality for interpretation. Therefore, extracting quantitative information from such images is of great clinical importance. The purpose of this work is automatic tracking of the motion of the MVA over the full cardiac cycle; specifically, tracking the mitral valve hinge points (MVHPs). This method can be useful on its own, but we mainly intend it to be part of a semi-automatic border detection approach (chapter 2), to improve the LV volume estimation. Given the septal and the lateral MVHPs in the first frame (fig. 3.1), e.g. by manual annotation, we desire to track them over the full cardiac cycle.

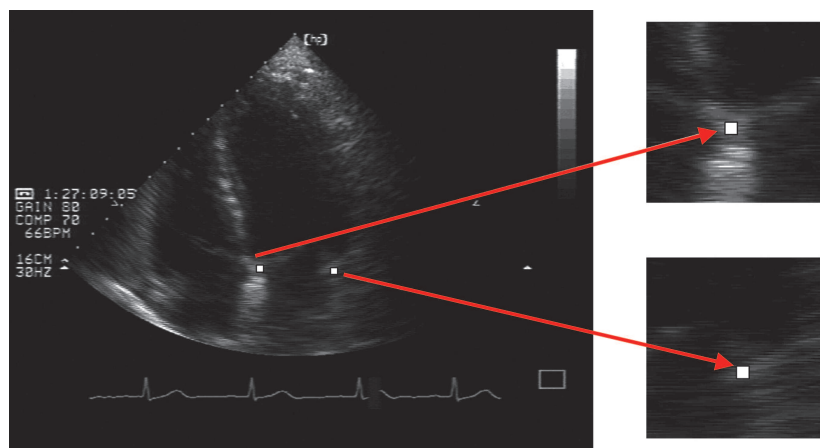


Figure 3.1: The white points represent the septal (left) and the lateral (right) MVHPs in the first frame

related work Common methods for evaluating the mitral annular motion are M-mode echocardiography [Unser et al. 1989; Willenheimer et al. 1999], two-dimensional (2D) echocardiography [Behar et al. 2004; DeCara et al. 2005; Eto et al. 2005], three-dimensional (3D) echocardiography [Flachskampf et al. 2000] and Doppler tissue

echocardiography [Rabben et al. 2000]. Unser et al. [1989] performed one-dimensional (1D) dynamic programming (DP) on M-mode echocardiograms (see section 1.2.1) for border detection. Rabben et al. [2000] implemented 1D DP on Doppler tissue echocardiograms combined with gray-scale M-mode for contour detection. The dominant drawback of M-mode and Doppler tissue echocardiography is that they detect the MVA motion only along a fixed line (angle dependency). DeCara et al. [2005] results for automated tracking of mitral annular displacement based on speckle tracking. Previous studies [Behar et al. 2004; Eto et al. 2005] suggested block matching combined with forward tracking for tissue tracking using 2D echocardiography. The main drawbacks of forward tracking are the sensitivity to small disturbances and tendency to drift away from the optimal path once an error has occurred.

To overcome such limitations, we propose a 2D echocardiography based tracking technique using multidimensional dynamic programming (MDP) combined with apodized block matching.

Materials and methods | 3.2

Blockmatching | 3.2.1

Block matching is a common technique for motion tracking in ultrasound data [Chen et al. 1995; Leung et al. 2006a]. Given a sequence of 2D echocardiographic images, the user selects the point to be tracked in the reference image (first image) and a region-of-interest (ROI) is defined around it (ROI_1). The displacement of a certain point is estimated by searching for $ROI_t(k, l)$ (with the same size as ROI_1) in the region-of-search (ROS) in the target frame (t) with the most similar gray level pattern to that of ROI_1 (see fig. 3.2). For each shift (k, l) the similarity of the patterns between ROI_1 and $ROI_t(k, l)$ is estimated by a cost function (matching criterion). The shifts (k, l) with respect to ROI_1 that correspond to good values of the cost function are likely displacement estimates [Behar et al. 2004; Leung et al. 2006a]. Three candidates for cost functions were considered:

region-of-interest
region-of-search

1. Sum of squared differences (SSD) of gray values between ROI_1 in the reference frame and $ROI_t(k, l)$ in the target frame. This cost function is optimal when it is minimal. The general formula for the SSD [Leung et al. 2006a],

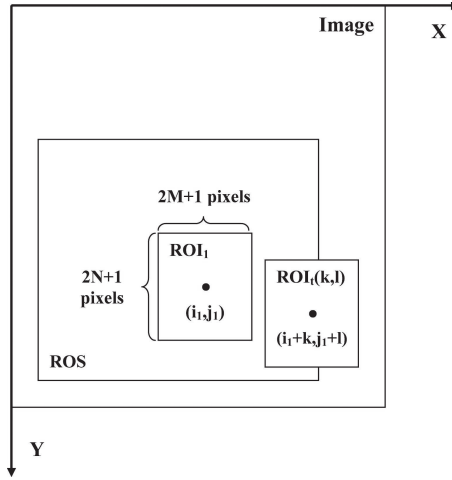


Figure 3.2: The block matching components

combined with the apodization kernel is:

$$SSD(k, l, t) = \sqrt{\sum_{j=j_1-N}^{j_1+N} \sum_{i=i_1-M}^{i_1+M} (|I_1(i, j) - I_t(i+k, j+l)| \cdot W(i, j))^2} \quad (3.1)$$

where $I_1(i, j)$ and $I_t(i, j)$ denote the pixel gray level at position (i, j) of the reference frame and the target frame respectively, $2M+1$ and $2N+1$ are the size of the ROI, (k, l) are the offsets of ROI_t within I_t with respect to I_1 and $W(i, j)$ is an apodization kernel that gives high relevance to central pixels.

2. Sum of absolute differences (SAD) of gray values between ROI_1 and $ROI_t(k, l)$. This cost function is optimal when it is minimal. The general formula for the SAD [Leung et al. 2006a], combined with the apodization kernel is:

$$SAD(k, l, t) = \sum_{j=j_1-N}^{j_1+N} \sum_{i=i_1-M}^{i_1+M} (|I_1(i, j) - I_t(i+k, j+l)| \cdot W(i, j)) \quad (3.2)$$

3. Normalized cross correlation (NCC) of ROI_1 and $ROI_t(k, l)$. This cost function is optimal when it is maximal. The general formula for the NCC [Bohs and

Trahey 1991], combined with the apodization kernel is:

$$NCC(k, l, t) = \frac{\sum_{j=j_1-N}^{j_1+N} \sum_{i=i_1-M}^{i_1+M} \mathcal{I}_1(i, j) \mathcal{I}_t(i, j, k, l)}{\sqrt{\sum_{j=j_1-N}^{j_1+N} \sum_{i=i_1-M}^{i_1+M} \mathcal{I}_1(i, j)^2 \sum_{j=j_1-N}^{j_1+N} \sum_{i=i_1-M}^{i_1+M} \mathcal{I}_t(i, j, k, l)^2}} \quad (3.3)$$

$$\mathcal{I}_1(i, j) = (I_1(i, j) - \bar{I}_1) \cdot W(i, j)$$

$$\mathcal{I}_t(i, j, k, l) = (I_t(i+k, j+l) - \bar{I}_t) \cdot W(i, j)$$

where \bar{I}_1 and \bar{I}_t indicate the mean values of ROI₁ and ROI_t, respectively. The NCC has the advantage that it is insensitive to local variations in the mean and standard deviation of the image gray level [Golemati et al. 2003]. For consistency with the other cost functions, we considered the cost function $1 - NCC(k, l, t)$, which is optimal when it is minimal.

Concepts of dynamic programming | 3.2.2

Dynamic programming (DP) is an optimal approach for solving variational problems by finding locally optimal solutions consecutively. DP algorithms provide an efficient way of finding an optimal path through a graph of nodes. In an image processing context, the graph is generally a matrix of image-related cost values ordered with root and leaves from left to right. The maximum distance between two nodes in consecutive columns, the step size, is predefined according to the desired connectivity. The task is to find a connective path through this matrix with minimal total cost. This is achieved by sweeping from left to right through the graph and finding for all nodes the lowest cumulative cost to reach this node from any of its predecessors in the previous column (for which the lowest cumulative cost is already known). Each element in the cumulative cost matrix corresponds to the minimal sum of costs to reach this point from the beginning of the matrix. In the last step, the optimal path is extracted by finding the minimal value in the last column and tracking back through minimal values over the cumulative cost matrix. The result is a global optimal path [Amini et al. 1990; Sonka et al. 1999; Üzümcü et al. 2006].

*graph search
technique*

cost matrix

back tracking

An example of DP search for a 1D path is illustrated in fig. 3.3. The matrix on the left is the cost matrix as derived from an image related cost function (e.g. block matching). Each term in the cost matrix represents a node with a given cost. The matrix on the right is the cumulative cost matrix derived from the original cost matrix when passing through it from left to right. The backtracking begins from the

minimal cumulative cost in the rightmost column and propagates to the left. The optimal path, which connects minimal cumulative costs per column, as calculated from the back-propagation, is shown in red.

multi-dimensional dynamic programming

In most cases, DP is applied in the way described above, resulting in an optimal path through a 2D array. In a tracking problem, the horizontal axis represents the consecutive time steps and the vertical axis represents a certain parameter, for example, 1D displacement. In our tracking problem, the purpose is to track two parameters simultaneously: horizontal and vertical displacement. This can be done by applying multidimensional dynamic programming (MDP) [Üzümcü et al. 2006], 2D DP in our case: finding a path through a stack of slices (a 3D data set), where each slice corresponds to the ROS filled with the values of the 2D cost function that was obtained from the block matching. 2D DP is illustrated in fig. 3.4.

A common variation of DP in tracking is forcing a path through a node. Certain points can be imposed to be on the path by setting the costs of all other nodes of a certain column (in the 1D case) or a certain slice (in the 2D case) to sufficiently high values [Sonka et al. 1999; Üzümcü et al. 2006]. In our case, the user specifies the positions of the MVHPs in the first frame. Next, they are tracked over the cardiac cycle by finding the optimal path that starts at this point.

3.2.3 | Tracking: MDP search combined with apodized block matching

manual initialization

The coordinates of the septal and the lateral MVHPs are determined in the first frame. After the user manually selects the two points representing the positions of the septal and lateral MVHPs, the automated tracking is started. An image patch around the manually chosen points in the first frame is used as the ROI to be matched. Block matching is applied by computing the cost function for each point in the ROS of each frame. In block matching in medical images, the size of the ROI is crucial. It should be large enough to identify a unique region, but small enough not to suffer too much from deformation of the block content over time. We want

3	1	4	4	3	1	5	9
0	2	8	6	0	2	9	9
5	5	1	7	5	5	3	10
6	9	0	2	6	14	5	5

Figure 3.3: Example of 1D DP. *left*) The cost matrix. *right*) The corresponding cumulative cost matrix with the optimal path marked in red

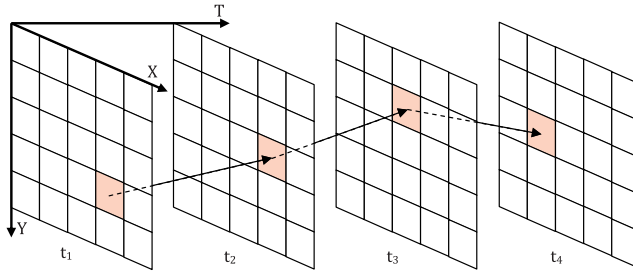


Figure 3.4: Example of 2D DP. Each slice represents the cost matrix at a certain frame. The optimal path is shown in red

to track the motion of the center pixel accurately. However, when using large rectangular blocks, the relative contribution of pixels far away from the center pixel becomes dominant. To limit this effect, we use an apodized block matching (as given by eqn. 3.1 to eqn. 3.3), meaning that within the summation over the ROI, the cost elements are multiplied by a 2D Gaussian kernel that gives higher weight to central elements rather than peripheral ones. The total ROI size is coupled to the width of the 2D Gaussian apodization kernel: it is chosen such that at least 90% of the summed apodization weights are included (the width of the ROI was chosen as 2×2 standard deviations of the Gaussian kernel). A path search using MDP is implemented to find the optimal locations of the septal and lateral MVHPs (nodes in the DP graph) separately over the cardiac cycle. The size of the ROS determines the dimensions of the DP graph. In this way, the horizontal and the vertical displacements of the MVHPs are tracked.

apodization

Parameter selection | 3.2.4

The performance of the method depends on the following parameters:

Width of smoothing filter In the preprocessing phase, the images are smoothed with a Gaussian filter in the spatial and the temporal domain. The variance (the width) of the filter determines the amount of smoothing. A Cartesian approach was followed rather than a polar one since the ROI is always in the same position and therefore Cartesian coordinates correspond well with polar coordinates. Moreover, the degradation of the image quality mainly occurs due to interlacing artifacts, which arise in Cartesian coordinates.

Apodized region-of-interest (ROI) size The ROI size (the size of the template to be matched) is chosen to be four times the standard deviation of the apodization

kernel in each direction. The ROI size determines the amount of information involved in the calculation of the costs.

Region-of-search (ROS) size The size of the search space should be large enough to accommodate the maximal displacement over the cardiac cycle without leading to an unnecessary computational load.

Step size The maximum allowed step size between two successive frames defines the maximum distance that the MVA can pass through. The step size should be large enough to handle the possible motion, especially the high velocities in early diastole. However, it should not be too large to maintain temporal and spatial continuity of the motion [Üzümcü et al. 2006; van Stralen et al. 2005].

The values of the step size and the ROS size were chosen based on normal values of MVA displacement [Alam and Hoglund 1992; Behar et al. 2004]. These were consistent with the results of the manual tracking performed on the 20 patients for the evaluation of the proposed method. The chosen values are given in table 3.1.

Table 3.1: The applied values for the step size in X and Y direction (SS_x and SS_y) and the ROS

	SS_x (pixels)	SS_y (pixels)	ROS (pixel ²)
Septal	2	6	61 × 91
Lateral	2	7	61 × 91

3.2.4.1 | Parameter optimization

A systematic optimization procedure was carried out to select the values for the width of the smoothing filter and of the apodized kernel that lead to the best results in the sense that the Euclidean distance is minimized. The parameter optimization process was performed in the following fashion: the initial step was trying many possible combinations of the parameter values in a wide range and the three types of cost functions. From this phase, we extracted the type of cost function that leads to the best results and we could define a narrower range of the parameter values that should be involved in the systematic optimization. Based on the results of the initial step, all possible combinations of smoothing filter with a standard deviation in the range [0, 3] and [0, 2] pixels with steps of 0.5 pixels in the spatial and the temporal domain, respectively ('-' means that no smoothing at all was applied) and apodization kernel with a standard deviation in the range [11, 19] pixels with steps of 2 pixels were examined. It is important to mention that the MDP search did not require any optimization procedure since it only depends on the ROS and the step size, which were determined beforehand.

Table 3.2: Optimal values of the parameters

	σ_x (pixels)	σ_y (pixels)	σ_t (frames)	α_x (pixels)	α_y (pixels)	ROS pixels ²
Septal	2.5	1	0.5	17	17	69 × 69
Lateral	-	-	-	17	13	69 × 53

σ_x , σ_y and σ_t are the standard deviations of the Gaussian filter in the spatial and the temporal domain, respectively, and α_x and α_y denote the standard deviations of the apodization kernel in the horizontal and vertical direction respectively. The region-of-interest (ROI) sizes are directly derived from α_x and α_y .

Data acquisition | 3.2.5

Single-beat apical four-chamber image sequences in 20 patients were recorded using a Hewlett-Packard Sonos 1500 or Sonos 2500 ultrasound system (Hewlett-Packard Inc, Andover, MA, USA) with a 2.5 MHz transducer. The patients were selected randomly from a database of 120 patients 3 days after acute myocardial infarction [Nijland et al. 2002]. Images were recorded on VHS videotape and digitized by a DT3152 frame grabber (Data Translation, Marlboro, MA, USA). The resolution was 768×576 pixels with pixel sizes ranging from 0.281×0.281 to 0.422×0.422 mm²/pixel. Cineloop images were acquired with the video frame rate of 25 Hz. All studies were acquired in apical position. To suppress high noise levels and interlacing artifacts in the raw data, a Gaussian filter (its parameters are given in table 3.2) was used to smooth the images in both the spatial and the temporal domain.

The tracking errors of three patients (for two of them in the lateral part and for the third one in the septal part) were detected as outliers and, therefore, they were excluded from this study. The failure of the tracking in two of them is attributable to the poor image quality of the sequences, resulting in a non discriminative ROI to be matched. As for the third outlier, after analyzing the results the two experts who performed the manual tracking agreed with the tracking results of the automated method rather than the averaged manual annotation. After excluding the three outliers from the study, the optimization was performed again with the remaining 17 patients (374 images in total).

outliers

3.2.6 | Data analysis

3.2.6.1 | Comparison with manual tracking

Since MVA tracking lacks “ground truth”, we compared the automatically computed positions with the positions indicated manually by two experts (JB and MvS). Both experts were constrained to begin the track from the same starting position and the rest of the cycle was annotated independently. The Euclidean distances between the computer generated annulus positions and the averaged manual positions were calculated. We used the average Euclidean distance as the distance measure.

3.2.6.2 | Comparison with other automatic tracking methods

The performance of the above automatic MDP-based procedure was evaluated relative to two other tracking methods:

1. Minimum tracking. This is the simplest approach for tracking problems based on block matching. The first step of this technique is applying block matching by calculating the costs using a single fixed template (ROI) for all frames (like in the proposed automatic procedure). After that, the optimal locations of the MVHPs are simply the local minima within the ROS for each frame, without enforcing any temporal continuity.
2. Forward tracking. Forward tracking is a common method that was used in previous studies [Behar et al. 2004; Eto et al. 2005; Golemati et al. 2003; Veronesi et al. 2006] for tissue tracking. In this algorithm block matching is applied and the minimum of the cost function is found in each frame separately. The template ROI_1 is updated in each frame and is set to be the content of ROI_t that minimized the cost function in the previous frame, as described in section 3.2.1. In this algorithm continuity is imposed by limiting the step size.

equal parameter settings The evaluation of the performance of these two methods was done using the same parameters as in the MDP-based method since they are independent of the tracking method. The parameters that were optimized are the width of the smoothing filter, which depends on the image quality and the size of the ROI, which is linked to the size of the anatomical structures to be tracked.

3.2.7 | Statistical analysis

Since we had manual tracking of two experts, we used the average of both of them as the best estimate of the true value. The difference between the tracking results

of the experts is a measure for the interobserver variability. Evaluating the performance of the proposed automated method by calculating the correlation between the manual tracking and the automated tracking is not enough in this context since high correlations do not necessarily mean that the two methods agree [Bland and Altman 1986]. Therefore, in addition to the linear regression analysis, we applied Bland-Altman analysis and measured the agreement between the MDP-based automated technique and the manual tracking. A paired t -test was applied to verify the significance of the bias. We compared between the interobserver variability and the errors of the automated method by examining the 95% confidence intervals of the limits of agreement. The 95% confidence intervals for the limits of agreement were calculated according to:

confidence interval

$$CI = 2S \pm t \sqrt{\frac{3S^2}{n}} \quad (3.4)$$

where S denotes the standard deviation, n is the number of observations, and t is the 0.05 critical value of the t -distribution with $n - 1$ degrees of freedom. Since we compare to the average of multiple manual values, we would underestimate the limits of agreement with respect to the manual method. Therefore, a corrected standard deviation [Bland and Altman 1986] was used in the calculations of the limits of agreement between the automatic technique and the manual tracking:

corrected standard deviation

$$S_c = \sqrt{S_e^2 + \frac{1}{4} S_m^2} \quad (3.5)$$

where S_c is the corrected standard deviation, S_e is the original standard deviation of the automated errors and S_m is the standard deviation of the differences between the tracking results of the two experts.

Results | 3.3

Parameter settings | 3.3.1

The NCC as a matching criterion yielded the best results of tracking both the septal and the lateral parts and, therefore, it was chosen as the cost function to be applied. The parameters obtained with the parameter optimization process are shown in table 3.2.

NCC

3.3.2 | Tracking results

Figure 3.5 shows the average displacement over all 17 patients as function of the relative phase of the cardiac cycle. It can be seen that good agreement between the displacements found by the MDP-based automated method and the manual method was obtained.

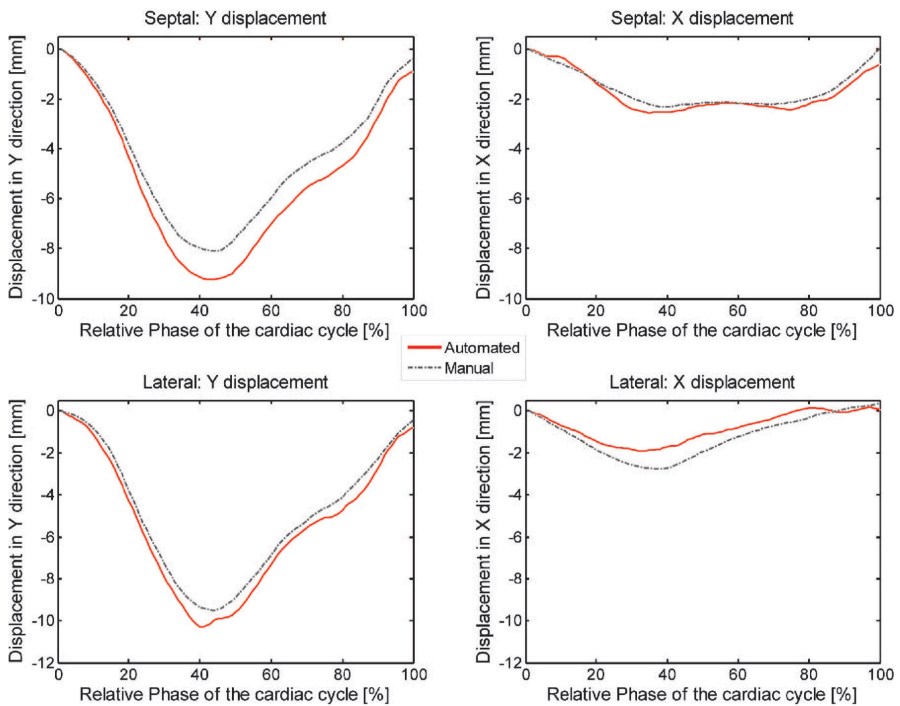


Figure 3.5: The average displacements over all 17 patients in *Y* (left) and *X* (right) directions in the septal and lateral MVHPs as function of the relative phase of the cardiac cycle in percentage

Table 3.3: The maximal excursion as calculated by the automated method and the manual method

$n = 17$	MDP-based automated method (mm)	Manual method (mm)
Septal	11.0 \pm 1.9	10.0 \pm 1.8
Lateral	12.4 \pm 2.8*	11.1 \pm 3.2

All the results are expressed as mean \pm standard deviation.

* Denotes an automated result which is significantly different ($p < 0.05$) from the manual result.

Maximal excursion | 3.3.3

The septal and the lateral MVHP maximal excursions over the cardiac cycle were calculated, the results are given in table 3.3. The MVA maximal excursion, which usually occurs at end systole, is the maximum distance between the initial MVHP (at end diastole) and the MVHP in all other frames. The first evaluation of the MDP-based automated method was done based on the maximal excursion results since it is related to other important clinical measures such as the ejection fraction and stroke volume [Alam and Hoglund 1992; DeCara et al. 2005; Eto et al. 2005; Willenheimer et al. 1999]. Bland-Altman plots of the difference between the calculated maximal excursions by both methods against the mean values of the methods are shown in fig. 3.6. In the septal part, no significant difference ($p > 0.05$) was found between the methods. As for the lateral part, a small but significant ($p < 0.05$) over-estimation of the automated method with a bias of 1.21 mm was found. However, it is important to mention that the maximal excursions in the lateral part, as indicated manually by both experts, were also found to be significantly different ($p < 0.05$) from each other.

Full cycle tracking | 3.3.4

The average MVA displacement errors (average Euclidean distance from the manual annotation) over all time samples and all 17 patients obtained from the proposed MDP-based automated procedure, from the forward tracking, from the minimum tracking and the interobserver variability are given in table 3.4. It can be clearly seen that the MDP-based tracking outperformed the forward and the minimum tracking.

High correlations were found ($p \ll 0.01$) between the displacement measure-

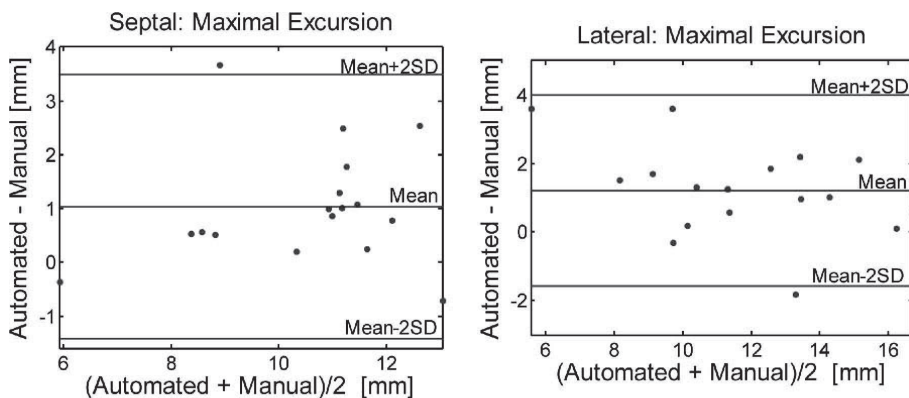


Figure 3.6: Bland-Altman plots of the difference between the maximal excursions in the septal (*left*) and the lateral (*right*) parts calculated by the automated method and those obtained by the manual method

Table 3.4: The errors obtained with the MDP-based automated method, the errors obtained from forward tracking, the errors obtained with the minimum tracking and the interobserver variability

$n = 17$	MDP-based tracking (mm)	Forward tracking (mm)	Minimum tracking (mm)	Interobserver variability (mm)
Septal	1.33 ± 0.86	2.14 ± 1.12	1.83 ± 2.19	1.43 ± 0.82
Lateral	1.66 ± 1.03	3.62 ± 2.21	4.21 ± 5.29	1.57 ± 0.94

All the results are expressed as mean \pm standard deviation.

ments obtained by the manual method and by the MDP-based automated method. The results, including the regression lines and the correlation coefficients, are shown in fig. 3.7

Bland-Altman plots for the agreement between the displacements obtained by our method and by those obtained manually are given in fig. 3.8 and fig. 3.9. The displacement is defined as the offset from the position in the first frame (end diastole). In these plots a negative displacement in Y direction is an upward movement and a negative displacement in X direction describes movement to the left. In the lateral part (fig. 3.9), Bland-Altman analysis showed a small but significant underestimation ($p < 0.05$) with a bias of 0.33 mm in the displacements in X direction

coordinate
system

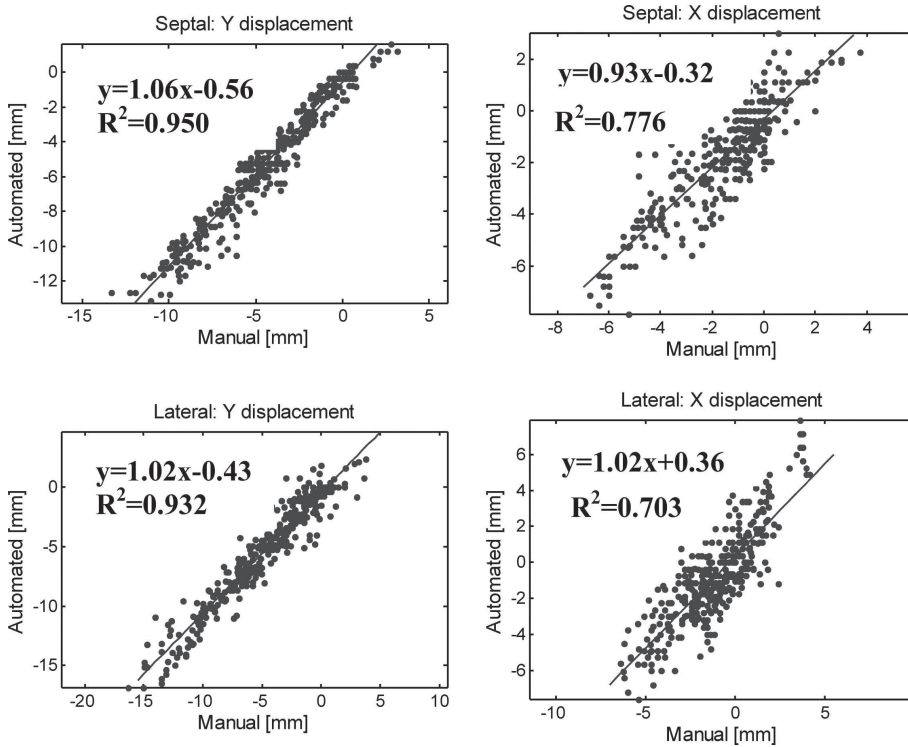


Figure 3.7: Results of the linear regression of the MVHPs displacement measurements obtained by the MDP-based automated method and by the manual method

and a small but significant overestimation with a bias of -0.52 mm in the displacements in Y direction. In the septal part (fig. 3.8) no significant difference ($p > 0.05$) was found.

The 95% confidence intervals of the limits of agreement, as calculated using eqn. 3.4, of both methods are shown in table 3.5. It can be seen that in the Y direction narrow limits of agreement for the difference between the two techniques were obtained although they are significantly different.

The computation time required for the proposed automatic method as well as those required for forward tracking and minimum tracking are given in table 3.6. The computation times shown are for full cycle tracking of the MVHPs on a notebook PC with an Intel Pentium M processor running at 1.73 GHz with 512 MB of RAM. However, we did not spend much effort in optimizing our method regarding

*computation
time*

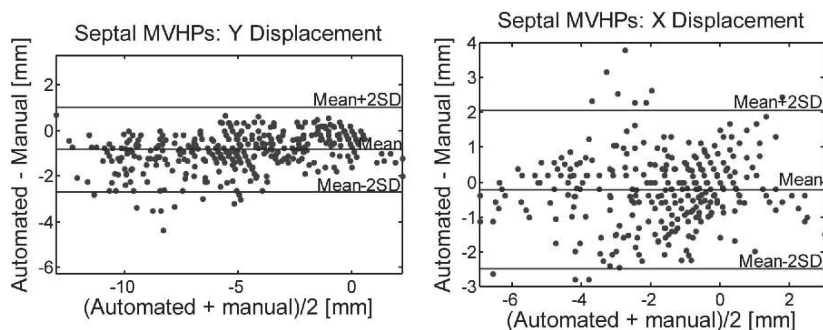


Figure 3.8: Bland-Altman plots of the differences between the automated and the manual displacements in the septal part, in both the horizontal (X) and vertical (Y) direction

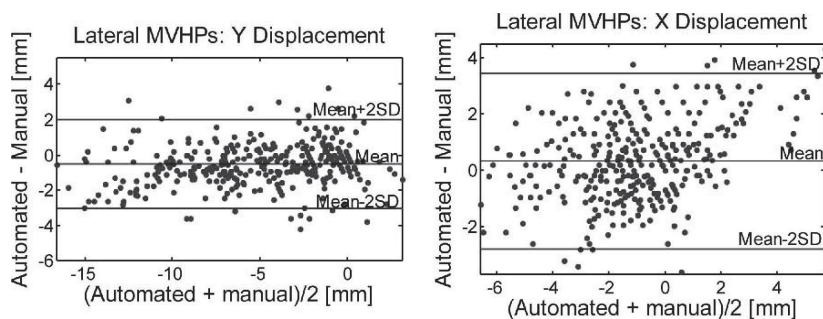


Figure 3.9: Bland-Altman plots of the differences between the automated and the manual displacements in the lateral part, in both the horizontal (X) and vertical (Y) direction

Table 3.5: The 95% confidence intervals for the limits of agreement of the errors in X direction and Y direction, respectively

$n = 17$	MDP-based tracking		Interobserver variability	
	X (mm)	Y (mm)	X (mm)	Y (mm)
Septal	2.28 ± 0.20	$1.86 \pm 0.16^*$	2.39 ± 0.21	1.63 ± 0.14
Lateral	3.12 ± 0.27	$2.55 \pm 0.22^*$	2.92 ± 0.26	2.09 ± 0.18

All the results are expressed as mean \pm standard deviation.

*Denotes an automated limit of agreement which is significantly different ($p < 0.05$) from the interobserver variability.

Table 3.6: Computation times per patient required for the three tracking methods

$n = 17$	MDP-based tracking (s)	Forward tracking (s)	Minimum tracking (s)
Computation time	161.1 ± 10.3	110.1 ± 9.7	143.7 ± 13.5

All the results are expressed as mean \pm standard deviation.

execution speed.

Discussion | 3.4

We developed a semi-automatic technique for tracking the MVA motion using MDP combined with apodized block matching. We applied this method on clinical quality VCR recorded data from 20 patients. We evaluated its feasibility on 17 patients, after excluding three patients due to poor image quality or ambiguity of the manual annotation of either the septal or the lateral MVHP. Tracking the MVA based on manual annotation is a cumbersome and tedious procedure with poor repeatability. To overcome this limitation, we propose a semi-automatic method that requires minimal user interaction. Relative to forward tracking and minimum tracking, the method is robust to noise and small disturbances.

Our method has several advantages for evaluating the MVA motion. First, it exploits the DP advantages: relatively insensitive to noise and small disturbances, efficient and producing a time continuous motion [Rabben et al. 2000; Sonka et al. 1999]. Another benefit from the MDP search is the 2D path derived from it. In this way, our technique is capable of evaluating the spatial displacement of the MVA in both the horizontal and the vertical direction over the full cardiac cycle. Second, it takes the advantages of block matching: robust against linear changes, fast and proven. Third, it is simple and can be performed off-line with a PC. In addition, the method has the benefits of 2D echocardiography: cheap relative to other image acquisition modalities, non-invasive, accessible and the images are produced in real time.

Previous studies [Alam and Hoglund 1992; DeCara et al. 2005; Eto et al. 2005; Willenheimer et al. 1999] reported that the MVA maximal excursion correlates well with LV function. The maximal excursions values obtained with our automated method agreed well with the values obtained with the manual method, consider-

advantages

MVA excursion

ing the inherent uncertainty of the manual drawing. Eto et al. [2005] developed an automated method, based on forward tracking, for tracking the MVA in high frame rate (greater than 60 Hz) cine-loop images of 2D echocardiography. They validated their method by comparing its results to those obtained by manual annotation in 3D echocardiography and reported an accuracy of 2.5 ± 1.8 mm (the average distance between the mean MVA excursion obtained by the automated method and the manual tracking). However, it is difficult to compare these results to those obtained by our method since they used a different “ground truth”.

*full cycle
tracking results*

The full cycle tracking errors obtained with the MDP-based automated technique were small (less than 2 mm, see table 3.4) and with clinically acceptable differences [Eto et al. 2005]. The tracking errors in the lateral part were larger than in the septal part. This can be explained by the fact that the lateral part is more difficult for tracking since the ROI has less clearly defined structures with lower echo level. Consequently, the interobserver variability was also larger in the lateral part than in the septal part. We found limits of agreement of less than 2 mm which is good given the uncertainty in our “ground truth”, which is expressed by the manual interobserver variability. Bland-Altman plots revealed good agreement between the displacements in X direction obtained by both methods. However, the limits of agreement of the displacements in Y direction obtained by the automated method were narrow but significantly different from those obtained by the manual method (see table 3.5). The wider limits of agreement in the X direction are attributable to the resolution, which is higher in the axial direction than in the lateral direction. Therefore, the resolution in the X direction, which is mainly governed by its lateral component, is worse and the limits of agreement are broader.

The displacement in the Y direction is clinically more valuable than in the X direction. No apparent correlation between the error and the average displacement was found (fig. 3.8 and fig. 3.9). This is a great advantage of the MDP-based automated method, which does not suffer from increasing errors even at large excursions.

The fact that the best results in the lateral part were obtained without smoothing the images implies again that in the lateral part there are no clear anatomical structures for tracking and the MVHP is tracked based on the speckles.

*related
techniques*

In our study, the MDP-based automated method outperformed the forward tracking and the minimum tracking while requiring comparable computation time (table 3.6). The forward tracking approach is fastest since the ROS is effectively smaller (limited by the step size), at the cost of finding a suboptimal solution. Unlike other echocardiography studies [Behar et al. 2004; Eto et al. 2005; Rabben et al. 2000], we used cine-loop images with low frame rate (25 Hz) compared with digital images. Forward tracking was reported to perform well in high quality images [Behar et al. 2004; Eto et al. 2005; Veronesi et al. 2006] but yielded poor results in

our case. This is attributable to the fact that in forward tracking once an error occurs it is emphasized since the new ROI is updated erroneously and the detected path drifts away from the true path. An important contribution to this problem is the change in appearance of the mitral valve leaflet due to opening and closing of the valve. Since this is the nature of the problems, applying our method on digital images with higher frame rate and better image quality would probably reduce the tracking errors. This is attributable to the fact that our method searches for globally optimal location of the MVHPs using MDP and uses apodized block matching to eliminate the dominant contribution from peripheral pixels in the ROI.

We chose the step size and the ROS size based on normal ranges of MVA displacement [Alam and Hoglund 1992; Behar et al. 2004] and, hence, they do not depend on the quality of the images used in this study. The performance of the method was not very sensitive to the choice of the parameters (smoothing filter size and ROI size) that were selected during the optimization procedure; the differences were only a few percent. However, these parameters depend on the image quality and hence we expect to find different values for other types of data, e.g. high-quality digital images.

*choice of
parameters*

We used the same parameters for tracking the entire data set. Better results may be achieved by selecting the ROI size for each patient separately based on the auto-correlation function of the system [Behar et al. 2004]. When implementing the proposed method on high quality digital images, its results may be further improved by using a nonlinear edge preserving filter to increase the signal to noise ratio (SNR) of the images while preserving important image features [Adam et al. 2006; Behar et al. 2004] instead of smoothing the data with a linear Gaussian filter as we did. Using nonlinear filters would probably improve the results in the septal part, where the MVHP is a strong reflector, rather than in the lateral part, where the MVHP is weaker (Behar et al. 2004). In our images with dominant interlacing artifacts, however, a smoothing filter is better than an edge preserving one.

*further
improvements*

Further work can be the extension of the method to 3D data. The MDP can be easily adapted to track the MVA in any long-axis slice of a four-dimensional data set (3D + time), or for detecting the complete mitral ring in a 3D set.

Limitations | 3.4.1

We analyzed only data obtained from patients with acute myocardial infarction. Although this subsample might not be fully representative, we do not see any reason why this method would not be suitable for normals or for patients with other pathologies, as long as no extreme kinematical changes are involved.

*patient
population*

The quality of the images was relatively low due to the VCR recorded data. Hence,

image quality

this study should only be seen as evidence for the feasibility of MDP-based automatic mitral valve tracking in VCR images. However, we developed this method on such relatively poor-quality data because we were aiming for a robust technique suitable for 3D ultrasound data, with an inherently lower quality than modern digital data. Since we wanted to use gross anatomical features rather than highly correlated speckle patterns in high frame rate, digital images with good SNR, the VCR images offered a good substrate.

The suitability of this technique for 3D echo still needs to be investigated, but its robustness is promising. We believe that our approach will also be useful on digital data, but further work on such data should be undertaken. At least, it will require a new parameter optimization process since the image quality influences the smoothing filter parameters.

3.5 | Conclusions

We developed a novel semi-automatic method based on MDP for tracking the MVA motion. This study showed that the technique is feasible and valuable in evaluating accurate MVA displacements. The method provides robust and efficient tracking with minimal user interaction and agrees well with manual MVHPs tracking even in low quality images.

| Acknowledgments

The authors acknowledge Dr. F. Nijland and Dr. O. Kamp (Department of Cardiology, VUMC, Amsterdam, the Netherlands) for supplying the data that was used in this study.
